Ab initio derived analytical fits of the two lowest triplet potential energy surfaces and theoretical rate constants for the $N(^4S)+NO(X\,^2\Pi)$ system

P. Gamallo, Miguel González,[a] and R. Sayós[b]
Departament de Química Física i Centre de Recerca en Química Teòrica, Universitat de Barcelona, C. Martí i Franquès 1, 08028 Barcelona, Spain

(Received 11 March 2003; accepted 2 May 2003)

This work presents two new analytical fits of the ground potential energy surface (PES) ($^3A''$) and the first excited PES ($^3A'$) involved in the title reaction, considering the N-abstraction (1) and the O-abstraction (2) reaction channels, and the reverse reaction (-1). The PESs are derived from *ab initio* electronic structure calculations by means of second-order perturbation theory on a complete active-space self-consistent-field wave function (CASPT2 method). Stationary points and extensive grids of *ab initio* points (about 5600 points for the $^3A''$ PES and 4900 points for the $^3A'$ PES) were fitted along with some diatomic spectroscopic data to better account for the experimental exoergicity. Thermal rate constants were calculated (200–5000 K) for all mentioned reaction processes by means of the variational transition-state theory with the inclusion of a semiclassical tunneling correction. Excellent agreement with the experimental data was observed for reaction (1) and its reverse, within all the temperature range, substantially improving the results derived from previous analytical PESs. The contribution of the $^3A'$ PES to the reaction rate constant (k_1) was small even at high temperatures (e.g., only 10.8% at 2500 K). Moreover, the main contribution to reaction rate constant (k_2) was due to the $^3A'$ PES, differing from what happens for reaction (1). The O-abstraction reaction channel accounts for a 3.0% of the total reaction ($k=k_1+k_2$) at 5000 K, consistent with the very limited experimental information available. © *2003 American Institute of Physics.* [DOI: 10.1063/1.1586251]

I. INTRODUCTION

The elementary gas-phase reaction of ground atomic nitrogen with nitric oxide,[1]

$$N(^4S)+NO(X\,^2\Pi)\rightarrow O(^3P)+N_2(X\,^1\Sigma_g^+)\Delta_r H^\circ_{0K} = -75.01 \text{ kcal/mol}, \quad (1)$$

and its reverse reaction are of interest in atmospheric chemistry. Reaction (1) is thought to be the dominant removal step for odd nitrogen in the upper stratosphere, the mesosphere, and the thermosphere of the Earth and, possibly, also in Mars and Venus.[2–4] The precision of the rate constants for this reaction over a wide range of temperatures [e.g., from 185 K in mesopause to approximately 1000 K at 250 km of altitude (upper thermosphere) (Ref. 5)] is of great interest for modeling the concentration of NO_x species in these atmospheric regions for different levels of solar activity. Moreover, this reaction has been also proposed as one important step to remove the NO molecules produced in some heterogeneous catalytic processes (e.g., in SiO_2-based materials) for airflow cases.[6] The reverse reaction is as well one of the two steps of the Zeldovich mechanism which produces NO, and it is very important for accurate modeling of thermochemical phenomena in rarefied atmospheric flows. A good understanding of the vibrationally and rotationally hot NO molecules produced by the reverse reaction is necessary to establish appropriately the heat flux on the thermal protection systems used in atmospheric reentry vehicles (e.g., American space shuttle, Japanese orbital reentry experiment, etc.).

Reaction (1) has been the object of abundant kinetic studies over several temperature ranges, but these studies present significant discrepancies, possibly due to its slight temperature dependence. Table I reports a brief summary of some of the main Arrhenius expressions for the experimental rate constants. A small activation energy (0.8–1.6 kcal/mol) or even a negative value (-0.2 to -0.3 kcal/mol) were reported in these works. Direct kinetic data for the reverse endothermic reaction have also been obtained mainly at high temperatures ($T>2000$ K),[8] and they are more coincident than in the case of the direct reaction.

There are very few experimental studies dealing with the dynamic properties of reaction (1) or about its reverse (-1). Very early studies showed a product N_2 average vibrational energy fraction of 0.25–0.28.[10,11] However, another past study indicated $75\%\pm5\%$ of the N_2 molecules appeared with $v'>4$.[12] To the best of our knowledge, there are no experimental dynamics studies on the reverse reaction. However, theoretical studies are available on both reactions. In earlier studies we presented several theoretical approaches for reaction (1), and we also gave a wide review of the main experimental and theoretical data that had been published for this reaction. We developed an analytical potential energy surface[13] (PES) based on limited *ab initio* information[14] for

[a]Electronic mail: miguel@qf.ub.es
[b]Electronic mail: r.sayos@qf.ub.es

 © 2003 American Institute of Physics

TABLE I. Experimental kinetic data for the $N(^4S)+NO\rightarrow O(^3P)+N_2$ reaction.

Reference	$k_1(T)$ (cm^3 $molecule^{-1}$ s^{-1})	T (K)	Method[a]
Clyne and McDermid[b]	$(8.2\pm1.4)\times10^{-11}e^{-410\pm120/T}$	298–670	DF-MS
Siskind and Rusch[c]	$1.6\times10^{-10}e^{-460\pm60/T}$	>300	review
Wennberg *et al.*[d]	$(2.2\pm0.2)\times10^{-11}e^{160\pm50/T}$	213–369	DF-RF
Baulch *et al.*[e]	$7.1\times10^{-11}e^{-790/T}$	1400–4000	review
DeMore *et al.*[f]	$2.1\times10^{-11}e^{100\pm100/T}$	200–400	review

[a]DF (discharge flow), MS (mass spectrometry), and RF (resonance fluorescence).
[b]Reference 7.
[c]Reference 2.
[d]Reference 3.
[e]Reference 8, with an error: $\Delta \log k=\pm0.2$. Data for its reverse reaction are also reported: $3.0\times10^{-10}e^{-38300/T}$ (1400–4000 K).
[f]Reference 9.

the ground $^3A''$ PES. In addition, we also performed dynamical studies on reaction (1) by means of the quasiclassical trajectory (QCT) method,[15] reduced quantum mechanical approaches,[16] and simple models.[17] Recently, QCT calculations on a new $^3A''$ PES,[18] which fitted the same aforementioned *ab initio* data,[14] but adding interpolated semiempirical points, reported good thermal rate constants for the 200–1000 K temperature range. In that work the authors considered the inclusion of a reactant statistical degeneracy factor excluding the NO spin-orbit correction (i.e., 3/16), missing in previous works. These authors also carried out a QCT study[19] on this reaction, taking into account the first excited PES ($^3A'$), previously fitted for the reverse reaction by other authors.[20] It was concluded that the excited PES became important for reaction (1) only at high energies (1–3 eV). Several theoretical studies on the reverse reaction, using these analytical PESs ($^3A''$ and $^3A'$), produced thermal rate constants and product energy distributions at very high temperatures (i.e., 3000–20 000 K), for both thermodynamic equilibrium[20] and nonequilibrium conditions.[21]

In addition to reaction (1), a second reaction channel involving the O-abstraction process,

$$N(^4S)+N'O(X\,^2\Pi)\rightarrow N'(^4S)+NO(X\,^2\Pi)\,\Delta_r H^\circ_{0K} = 0 \text{ kcal/mol}, \quad (2)$$

can be produced. There is almost no information about it. Some experiments[22,23] at very high energies with ^{13}N and pure NO have indicated that reaction channel 2 yielding ^{13}NO could account for up to a 20% of the total reactivity of this system, though with the possible contribution of the first excited states of nitrogen [$N(^2D, ^2P)$]. Nevertheless, there are neither kinetic nor dynamic data about this reaction.

In a recent study of our own (hereafter called paper I),[24] we have made an extensive *ab initio* characterization of the stationary points of the lowest $^3A''$ and $^3A'$ PESs. According to this study, reaction (1) should be much more important than reaction (2), which should only contribute to reactivity at high collision energies (e.g., over 30 kcal/mol). Moreover, we confirmed that the $^3A''$ PES had no energy barrier for reaction (1) and that the $^3A'$ PES had an energy barrier (TS1) much lower than the previous *ab initio* reported value.[14] Both PESs showed the presence of a minimum (MIN1) and a transition state (TS2) in the minimum energy path (MEP) for reaction (2).

Here we present new analytical PESs for both $^3A''$ and $^3A'$ states, based on the high-level *ab initio* data published in paper I, along with additional grids of *ab initio* points now calculated. These new PESs will provide better kinetic and dynamical data, and also will allow a deeper understanding of the two reaction channels involved in the title reaction. Furthermore, these PESs will be useful in the study of the reverse reaction in the nonequilibrium conditions of atmospheric reentry vehicles.

This paper is organized as follows: the *ab initio* method, the fitting procedure, and the derived analytical PESs are described in Sec. II, several variational transition-state theory calculations on thermal rate constants are presented in Sec. III, and finally Sec. IV contains the main concluding remarks.

II. ANALYTICAL POTENTIAL ENERGY SURFACES

A. *Ab initio* molecular structure and surface fitting methods

We have carried out the calculation of grids of *ab initio* points for both PESs following the main *ab initio* method used in paper I.[24] Thus the complete active-space self-consistent-field (CASSCF) method[25,26] was used, always including the lowest root in C_s symmetry for both triplet PESs (i.e., $^3A'$ and $^3A''$). An active space comprising ten electrons in nine orbitals [i.e., CAS(10,9)] and the standard correlation-consistent cc-pVTZ Dunning's basis set[27] were applied in all calculations. Results obtained in paper I (Ref. 24) showed that this *ab initio* level was accurate enough, and the computer time was also reasonable to compute a large number of points for both reaction channels. The dynamical correlation energy was included by performing second-order perturbation theory calculations (CASPT2) over the CASSCF wave function using the G2 variant.[28] All calculations were carried out by means of the MOLCAS 4.1 program.[29]

The analytical representations of the PESs are based on a many-body expansion[30] for the NN′O system. In both cases this expansion can be written as

$$V(R_1,R_2,R_3)=V^{(2)}_{NN'}(R_1)+V^{(2)}_{N'O}(R_2)+V^{(2)}_{NO}(R_3)+V^{(3)}_{NN'O}(R_1,R_2,R_3), \quad (3)$$

where $V^{(2)}$ and $V^{(3)}$ are the two- and three-body terms, respectively, and R_1, R_2, and R_3 are the NN′, N′O, and NO distances, respectively. The one-body $V^{(1)}$ terms have been omitted here because all the diatomic molecules dissociate into atoms in their ground electronic states [$N(^4S)+N'(^4S)+O(^3P)$]. The two-body terms (diatomic potential energy curves) have been fitted using an extended-Rydberg potential up to third or fifth-order,

TABLE II. Optimal parameters for the $^3A''$ and $^3A'$ analytical PESs.

Two-body terms[a] Species	a_1	a_2	a_3	a_4	a_5
NO($X\,^2\Pi$)[b]	4.3205	1.6392	1.4946		
	6.1958	11.1408	9.2570	6.9823	19.6021
$N_2(X\,^1\Sigma_g^+)$[b]	5.2376	6.3901	6.3676		
	3.7790	−0.2694	−0.6111	−1.9853	0.8992

Three-body term[c]	$^3A''$	$^3A'$		$^3A''$	$^3A'$		$^3A''$	$^3A'$
c_{000}	7.4166	4.6391	c_{040}	−21.3448	−0.3493	c_{330}	−9.0038	−4.3822
c_{100}	6.2889	−0.4166	c_{022}	−85.2948	−13.3716	c_{312}	14.2243	6.8153
c_{010}	−0.7505	−2.2228	c_{004}	−3.0718	−7.5467	c_{240}	7.2399	2.1739
c_{200}	14.4281	6.7267	c_{500}	8.9826	4.7293	c_{222}	−47.4708	−26.2565
c_{110}	−8.2247	−4.4265	c_{410}	−15.3167	−16.2801	c_{204}	11.6069	8.0923
c_{020}	12.8055	3.5126	c_{320}	45.2012	19.8618	c_{150}	4.3132	−1.8714
c_{002}	−8.4511	3.1430	c_{302}	−23.2229	−15.1099	c_{132}	45.2050	19.3009
c_{300}	13.4837	4.7954	c_{230}	−31.3627	−11.8867	c_{114}	7.7826	4.2956
c_{210}	−38.7067	−9.4334	c_{212}	74.0436	44.9758	c_{060}	−0.1399	−0.1853
c_{120}	32.9097	4.8414	c_{140}	−12.7283	4.6653	c_{042}	−5.4665	−2.1531
c_{102}	−30.9122	6.0499	c_{122}	−150.0063	−43.1208	c_{024}	−23.4852	−11.7849
c_{030}	12.9529	−3.2647	c_{104}	13.6449	−9.8957	c_{006}	−3.8063	−0.1736
c_{012}	12.7846	−3.9775	c_{050}	5.4116	−0.0326			
c_{400}	14.8181	4.9946	c_{032}	69.8672	19.0150	γ_1	2.5067	2.3806
c_{310}	−48.1654	−12.3015	c_{014}	41.4556	20.2721	γ_2	3.0405	2.1632
c_{220}	71.4660	13.4089	c_{600}	1.8306	1.0226			
c_{202}	−34.5457	−18.0314	c_{510}	−0.3524	−7.0602	R_1°	2.0980	1.9680
c_{130}	−7.0240	−11.3859	c_{420}	3.0192	8.6305	R_2°	1.3231	1.4789
c_{112}	74.1564	19.3841	c_{402}	−12.2485	0.3747	R_3°	1.3231	1.4789

[a]The dissociation energies and the equilibrium distances used in the fits are given in Table III.
[b]Extended Rydberg coefficients used for the $^3A''$ PES (first row) and the $^3A'$ PES (second row).
[c]Units are c_{ijk} (eV Å$^{-(i+j+k)}$), γ_i (Å^{-1}), R_i° (Å), and a_i (Å^{-i}), where $R_1=R_{NN'}$, $R_2=R_{N'O}$, and $R_3=R_{NO}$.

$$V^{(2)}(R)=-D_e\left(1+\sum_{i=1}^{n\leqslant 5} a_i\rho^i\right)e^{-a_1\rho}, \tag{4}$$

where D_e and R_e are the equilibrium dissociation energy and the equilibrium bond distance of each diatomic molecule, respectively, and ρ is defined as being equal to $R-R_e$.

The three-body term is a product of a sixth-order polynomial $P(S_1,S_2,S_3)$ and a range function $T(S_1,S_2,S_3)$, both expressed in terms of symmetry-adapted coordinates (S_1,S_2,S_3):

$$V^{(3)}_{NN'O}(S_1,S_2,S_3)=P(S_1,S_2,S_3)T(S_1,S_2,S_3), \tag{5}$$

with

$$P(S_1,S_2,S_3)=\sum_{i,j,k=0}^{0\leqslant i+j+k\leqslant 6} c_{ijk}S_1^iS_2^jS_3^k, \tag{6}$$

with i, j, and k being positive integer numbers and

$$T(S_1,S_2,S_3)=\prod_{i=1}^{3}\left[1-\tanh\left(\frac{\gamma_iS_i}{2}\right)\right]. \tag{7}$$

The range function vanishes the three-body term whenever one of the three atoms is separated from the other two. The symmetry-adapted coordinates used were

$$S_1=\rho_1,$$

$$S_2=\frac{1}{\sqrt{2}}(\rho_2+\rho_3), \tag{8}$$

$$S_3=\frac{1}{\sqrt{2}}(\rho_2-\rho_3),$$

and $\rho_i=R_i-R_i^\circ$ with $(R_1^\circ,R_2^\circ,R_3^\circ)$ defining a reference C_{2v} structure. The use of these coordinates guarantees the permutational NN′ symmetry of the analytical PESs.

The two-body parameters (a_i) were optimized by means of a nonlinear least-squares procedure,[31] while the three-body parameters (c_{ijk} and γ_i) were optimized by a weighted nonlinear least-squares method.[32] In both cases we follow a similar strategy as in our previous works [e.g., N(^2D)+NO (Ref. 33). N(^2D)+O_2 (Ref. 34), or N(^4S)+O_2 (Ref. 35)].

B. Analytical representation of the $^3A''$ PES

A total of 30 *ab initio* points [CASPT2(10,9) G2/cc-pVTZ] calculated for each diatomic molecule (supermolecule calculations for NO and N_2) have been fitted by using an extended-Rydberg potential curve [Eq. (4)] up to third order for the two diatomic curves used in the $^3A''$ PES and up to fifth-order for the $^3A'$ PES. The spectroscopic R_e and D_e values[36] were used for both curves. The final root-mean-square deviation (RMSD) of the fit in each diatomic energy curve was below 0.8 kcal/mol (with three parameters) and 0.4 kcal/mol (with five parameters) for both molecules. The

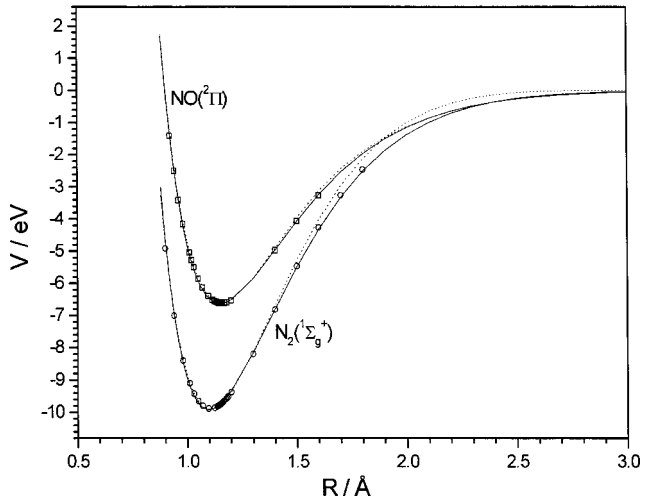

FIG. 1. *Ab initio* [CASPT2(10,9) G2/cc-pVTZ] diatomic points for the NO($X\,^2\Pi$) and the $N_2(X\,^1\Sigma_g^+)$ molecules. The lines show the analytical fit which reproduces also the experimental R_e and D_e, by using a third-order extended-Rydberg potential (dotted lines, for the $^3A''$ PES) or by using a fifth-order extended-Rydberg potential (solid lines, for the $^3A'$ PES).

optimal parameters are shown in Table II. Although both curves for each molecule are similar (Fig. 1), it was necessary improve the first diatomic fit (with three parameters), because the small differences at long distances (mainly for N_2) were significant to remove spurious minima during the fit of the second PES ($^3A'$). The spectroscopic constants of the diatomic molecules derived from the optimal analytical curves are summarized in Table III, which compared very well with the experimental data, only with small differences for both analytical curves.

A total of 5630 *ab initio* points [CASPT2(10,9) G2/cc-pVTZ] have been computed in different regions of the $^3A''$ PES to be used in the analytical fit, as summarized below:

(a) 3917 points for the NN′O region (N′-abstraction channel) distributed within the following grids:

$100° \leqslant \angle \mathrm{NN'O} \leqslant 140°$ for $0.9\ \text{Å} \leqslant R_{\mathrm{NN'}} \leqslant 4.5\ \text{Å}$ and $0.9\ \text{Å} \leqslant R_{\mathrm{N'O}} \leqslant 4.5\ \text{Å}$ (general and MEP),

$80° \leqslant \angle \mathrm{NN'O} \leqslant 180°$ for $2.1\ \text{Å} \leqslant R_{\mathrm{NN'}} \leqslant 4.5\ \text{Å}$ and $1.0\ \text{Å} \leqslant R_{\mathrm{N'O}} \leqslant 1.25\ \text{Å}$ (entrance valley),

$80° \leqslant \angle \mathrm{NN'O} \leqslant 180°$ for $0.9\ \text{Å} \leqslant R_{\mathrm{NN'}} 1.2\ \text{Å}$ and $1.8\ \text{Å} \leqslant R_{\mathrm{N'O}} \leqslant 4.5\ \text{Å}$ (exit valley).

(b) 1713 points for the NON′ region (O-abstraction channel) distributed within the following grids:

$90° \leqslant \angle \mathrm{NON'} \leqslant 180°$ for $0.9\text{Å} \leqslant R_{\mathrm{NO}} \leqslant 4.5\ \text{Å}$ and $0.9\ \text{Å} \leqslant R_{\mathrm{ON'}} \leqslant 4.5\ \text{Å}$ (general and MEP),

$80° \leqslant \angle \mathrm{NON'} \leqslant 150°$ for $2.3\ \text{Å} \leqslant R_{\mathrm{NO}} \leqslant 4.5\ \text{Å}$ and $1.0\ \text{Å} \leqslant R_{\mathrm{ON'}} \leqslant 1.25\ \text{Å}$ (entrance or exit valley),

$100° \leqslant \angle \mathrm{NON'} \leqslant 108°$ for $1.15\ \text{Å} \leqslant R_{\mathrm{NO}} \leqslant 1.6\ \text{Å}$ and $1.15\ \text{Å} \leqslant R_{\mathrm{ON'}} \leqslant 1.6\ \text{Å}$ (MIN1 and TS2 regions).

A small modification was introduced in the *ab initio* data in order to reproduce as accurately as possible the experimental diatomic dissociation energies and, hence, the exoergicity of reaction (1). As both *ab initio* values[24] were smaller than their experimental values, a uniform and first energy shift corresponding to the NO difference was introduced in all the points of the entrance valley (approximately from the line $R_{\mathrm{NO}} < 1.8\ \text{Å}$) for reaction (1) and for all points calculated for reaction (2). Afterward, an additional energy shift was added to the points of the exit valley (approximately from line $R_{\mathrm{NO}} > 1.8\ \text{Å}$) for reaction (1). This procedure was made trying to preserve as much as possible the original *ab initio* shape of the PES. All these *ab initio* points along with the first-order partial derivatives with respect to both distances and its angle for MIN1 and TS2 were used in a weighted nonlinear least-squares method[32] to obtain the optimal fit. The weights used were equal to 1 for almost all points, with the exception of the grids corresponding to the entrance and exit valleys, and also in the first-order partial derivatives, where we used weights between 50 and 100.

TABLE III. Spectroscopic constants of the diatomic molecules.

Molecule	R_e (Å)	D_e (kcal/mol)	ω_e (cm^{-1})	$\omega_e x_e$ (cm^{-1})	B_e (cm^{-1})	α_e (cm^{-1})	$\overline{D_e}$ (cm^{-1})
NO($X\,^2\Pi$)							
Analytical fit[a]	1.1508	152.53	1900.4	16.348	1.6861	1.99×10^{-2}	5.40×10^{-6}
			1947.3	16.128	1.6861	1.60×10^{-2}	5.16×10^{-6}
Experimental[b]	1.1508	152.53	1904.2	14.075	1.6720	1.71×10^{-2}	5.47×10^{-6}
$N_2(X\,^1\Sigma_g^+)$							
Analytical fit[a]	1.0977	228.41	2374.8	15.757	1.9754	2.15×10^{-2}	5.72×10^{-6}
			2388.2	14.582	1.9751	1.71×10^{-2}	5.66×10^{-6}
Experimental[b]	1.0977	228.41	2358.6	14.324	1.9982	1.73×10^{-2}	5.76×10^{-6}

[a]Spectroscopic parameters from the diatomic fits for the $^3A''$ PES (first row) and the $^3A'$ PES (second row).
[b]Experimental data of NO($X\,^2\Pi_{1/2}$) and $N_2(X\,^1\Sigma_g^+)$ from Ref. 36.

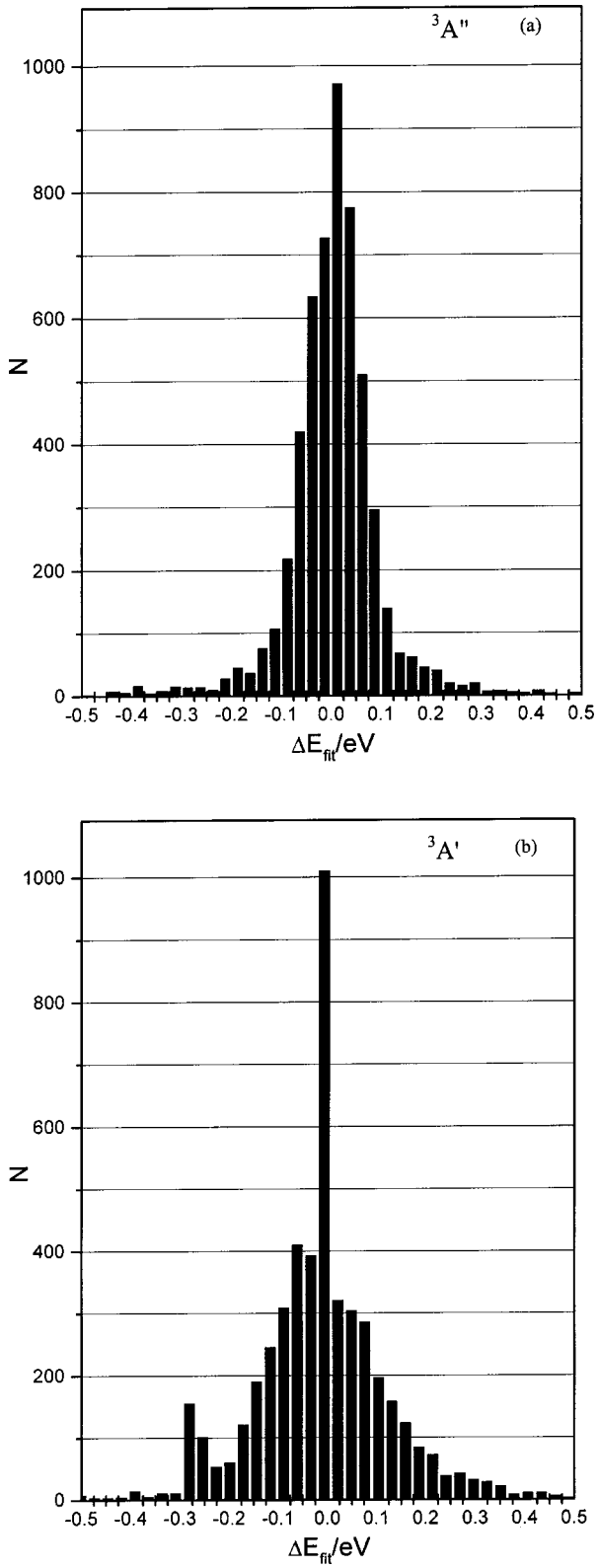

FIG. 2. Distribution of the energy deviations ($\Delta E_{\text{fit}}=E_{\text{analytical}}-E_{ab\ initio}$) for both analytical PESs: (a) $^3A''$ (5630 points) and (b) $^3A'$ (4901 points).

We employed as initial reference structure the C_{2v} geometry used in our first work ($R_1^\circ=2.17$ Å, $R_2^\circ=R_3^\circ=1.96$ Å) (Ref. 13) and which was slightly optimized by trial and error to improve the final fit. The optimal 55 three-body parameters (c_{ijk}, γ_i and R_i°) are shown in Table II. The final RMSD for the $^3A''$ surface was equal to 1.44 kcal/mol for the NN′O region and 2.59 kcal/mol for the NON′ insertion region. The global RMSD for this surface was 1.80 kcal/mol. These RMSDs are lower than the estimate errors of the *ab initio* method, as were shown in paper I (Ref. 24) [e.g., the *ab initio* D_e (NO) value was equal to 146.15 kcal/mol compared to the experimental value of 152.53 kcal/mol]. Figure 2(a) shows the energy deviations of the fit (i.e., $\Delta E_{\text{fit}}=E_{\text{analytical}}-E_{ab\ initio}$), which show a quite narrow distribution supporting the goodness of the fit. On the other hand, the in principle larger RMSD for the NON′ region is really much lower in relative terms for this quite repulsive PES region related with the O-abstraction channel. Table IV shows the properties of the stationary points fitted in this region of the PES (TS2 and MIN1), which are located at very high energies over reactants. There is a good agreement between the *ab initio* properties reported in paper I for these stationary points and the values of the fit shown in Table IV, regardless of the main effort was focused in the fit of the NN′O region, because reaction (1) was the principal reaction channel due to the absence of energy barrier along the MEP. Thus the fitted TS2 and MIN1 were located only 0.7
kcal/mol (1.7% of error) and 2.3 kcal/mol (6.2% of error) below their *ab initio* values,[24] respectively. Figure 3 presents some equipotential energy curves corresponding to the $^3A''$ PES, where it becomes evident the absence of an energy barrier for reaction (1) [see Figs. 3(a) and 3(b)]. In Fig. 3(c) we can observe TS2 and MIN, which are energetically and geometrically very close. This proximity produced some difficulties in their characterization, especially for the harmonic vibrational frequency ω_3 (asymmetric stretching of b_2 symmetry). Several intrinsic reaction coordinate (IRC) calculations were carried out to make sure the MEPs that are schematically shown in Fig. 4(a) for both reaction channels.

C. Analytical representation of the $^3A'$ PES

We have followed for the $^3A'$ PES the same procedure indicated in previous section for the $^3A''$ PES. In this case, as was explained before, the diatomic curves were fitted using a fifth-order extended Rydberg (Table II). We used as initial reference structure the optimal geometry found for the $^3A''$ PES, which was slightly optimized by trial and error.

A total of 4901 *ab initio* points [CASPT2(10,9) G2/cc-pVTZ] have been calculated in different regions of the $^3A'$ PES to be used in the analytical fit, as summarized below:

(a) 2614 points for the NN′O region (N′-abstraction channel) distributed within the following grids:

$80° \leqslant \angle \text{NN}'\text{O} \leqslant 180°$ for 0.9 Å $\leqslant R_{\text{NN}'} \leqslant 4.5$ Å

and 0.9 Å $\leqslant R_{\text{N}'\text{O}} \leqslant 4.5$ Å (general and MEP),

$112° \leqslant \angle \text{NN}'\text{O} \leqslant 117°$ for 1.9 Å $\leqslant R_{\text{NN}'} \leqslant 2.05$ Å

and 1.14 Å $\leqslant R_{\text{N}'\text{O}} \leqslant 1.18$ Å (TS1 region).

(b) 2287 points for the NON′ region (O-abstraction channel) following the ranges:

$90° \leqslant \angle \text{NON}' \leqslant 180°$ for 0.9 Å $\leqslant R_{\text{NO}} \leqslant 4.5$ Å

and 0.9 Å $\leqslant R_{\text{ON}'} \leqslant 4.5$ Å (general and MEP),

TABLE IV. Properties of the stationary points located on the $^3A''$ and $^3A'$ analytical PESs.

Stationary points	$R_{e(NO)}$ (Å)[a] $R_{e(NN')}$ (Å)	$R_{c(N'O)}$ (Å)	<NON′ (deg)[a] <NN′O (deg)	ω_i (cm^{-1})[b]			ΔE (kcal mol^{-1})[c]
$^3A''$ PES							
TS2	1.3965	1.2609	102.01	299.22	1299.14	374.71i	40.45 (40.02)
MIN1	1.3218	1.3218	97.13	375.39	1274.70	41.54[d]	39.25 (38.95)
$^3A'$ PES							
TS2	1.6892	1.2008	115.01	445.72	1542.79	609.78i	27.33 (27.45)
MIN1	1.2921	1.2921	114.13	530.96	1105.97	1234.42	13.87 (15.19)
TS1	1.9755	1.1571	115.21	428.07	1793.61	380.27i	8.35 (8.74)
TS1[e]	1.8913	1.1690	116.5	438	1648	544i	14.4 (14.7)

[a]Variables used for the NON′ structures: (top) TS2, MIN1, and for the NN′O structures. (bottom) TS1.
[b]Harmonic vibrational frequencies: (a) NON′-C_s: ω_1 (NON′ bend., a′), ω_2 (ON′ str., a′), ω_3 (NO str., a′) respectively; (b) NON′-C_{2v}: ω_1 (NON′ bend., a_1), ω_2 (sym. str., a_1), ω_3 (asym. str., b_2), respectively (YZ taken as the molecular plane); (c) NN′O-C_s: ω_1 (NN′O bend., a′), ω_2 (N′O str., a′), and ω_3 (NN′ str., a′), respectively. Masses of the most abundant isotopes were used. ^{14}N and ^{16}O.
[c]Energy respect to $N(^4S)+N'O$. The value corrected with the difference of zero point energies is shown in parentheses.
[d]This frequency has an estimated error of ±100% due to its difficult numerical characterization (very flat surface).
[e]Properties of a previous analytical fit (Ref. 20).

$$121° \leqslant \angle NON' \leqslant 127° \quad \text{for} \quad 1.1\ \text{Å} \leqslant R_{NO} \leqslant 1.35\ \text{Å}$$
$$\text{and} \quad 1.25\ \text{Å} \leqslant R_{ON'} \leqslant 2.0\ \text{Å}$$
$$(\text{MIN1 and TS2 regions}).$$

Here we used the same correction in the *ab initio* data as for the $^3A''$ PES. These *ab initio* points with weight equal to 1 (excepting the grid around TS1 that has a weight of 1000), together with the first-order partial derivatives with respect to the internal coordinates of TS1, MIN1, and TS2 with weight 100, were used in the weighted nonlinear least-squares method to obtain the optimal analytical fit. The final RMSD for the $^3A'$ surface was the following: 1.61 kcal/mol for the NN′O region and 2.85 kcal/mol for the NON′ region, with a global RMSD of 2.28 kcal/mol. Figure 2(b) shows the distribution of deviations for this fit, which is somewhat poorer than that for the $^3A''$ PES. Figure 5 shows some equipotential curves corresponding to the $^3A'$ PES, where is possible to see the transition state TS1 [Figs. 5(a) and 5(b)] and TS2 and MIN1 [Fig. 5(c)]. The properties of the different stationary points are depicted in Table IV. The analytical $^3A'$ PES reproduces very well the *ab initio* TS1 properties [e.g., to be compared with the *ab initio* geometry $R_{NN'}=1.9680$ Å, $R_{N'O}=1.1578$ Å, $\angle NN'O=116.04°$, $\Delta E^{\neq}=8.38$ kcal/mol (Ref. 24)] which is the most important stationary point. These results can also be compared with a previous analytical PES (Ref. 20) based on limited *ab initio* data, which had a larger energy barrier and a longer NN distance (see Table IV). The lowering of the energy barrier was discussed in paper I (Ref. 24) and justified due to the importance of the N and O 2*s* electron correlation, omitted in early *ab initio*[14] studies. Furthermore, the strengthening of the NN distance was also observed in similar studies [e.g., $N(^4S)+O_2$ (Ref. 37)], when the geometry optimization was carried out directly by including the dynamical correlation energy.[24]

The quality of this PES fit is a bit worse for the TS2 and MIN1 structures. Nevertheless, the errors in their fitted energies were lower than a 2% of the corresponding *ab initio* values. Figure 4(b) presents schematically the MEPs corresponding to both reaction channels. It can be observed by comparison with the MEPs of the $^3A''$ PES that the second reaction channel becomes more accessible than for the $^3A''$ PES, although still at high temperatures.

III. VARIATIONAL TRANSITION-STATE THERMAL RATE CONSTANTS

Thermal rate constants for both reaction channels of $N(^4S)+NO(X\,^2\Pi)$ and also for the reverse reaction have been calculated within the 200–5000 K and 600–5000 K temperature intervals, respectively. We have considered different levels of the variational transition-state theory[38] (VTST), as implemented in the POLYRATE code.[39] The rate constant values finally presented were the improved canonical (ICVT) ones with a microcanonical optimized multidimensional tunneling correction (μOMT) for reaction (1) and its reverse and the ICVT ones with a small curvature tunneling correction (SCT) for the O-abstraction reaction. For this latter reaction this tunnel correction was the only acceptable one, due to the problems generated by the curvature of the MEP, with the presence also of the MIN1 and the two equivalent TS2s.

To calculate the total thermal rate constants for all reactions, we have used the two PESs ($^3A''$ and $^3A'$) that can contribute to reactivity within the temperature range studied. Moreover, we have also considered a spin-orbit correction as in recent similar studies,[33,35] to take into account the two NO reactant spin-orbit states for reactions (1) and (2). Thus, the electronic partition function $[Q(T)]$ of $NO(X\,^2\Pi)$ is given by

$$Q^{\text{elec}}_{NO(^2\Pi)}(T)=g(^2\Pi_{1/2})+g(^2\Pi_{3/2})e^{-\Delta/RT}, \tag{9}$$

where $g(^2\Pi_{1/2})$ and $g(^2\Pi_{3/2})$ are both equal to 2, and the

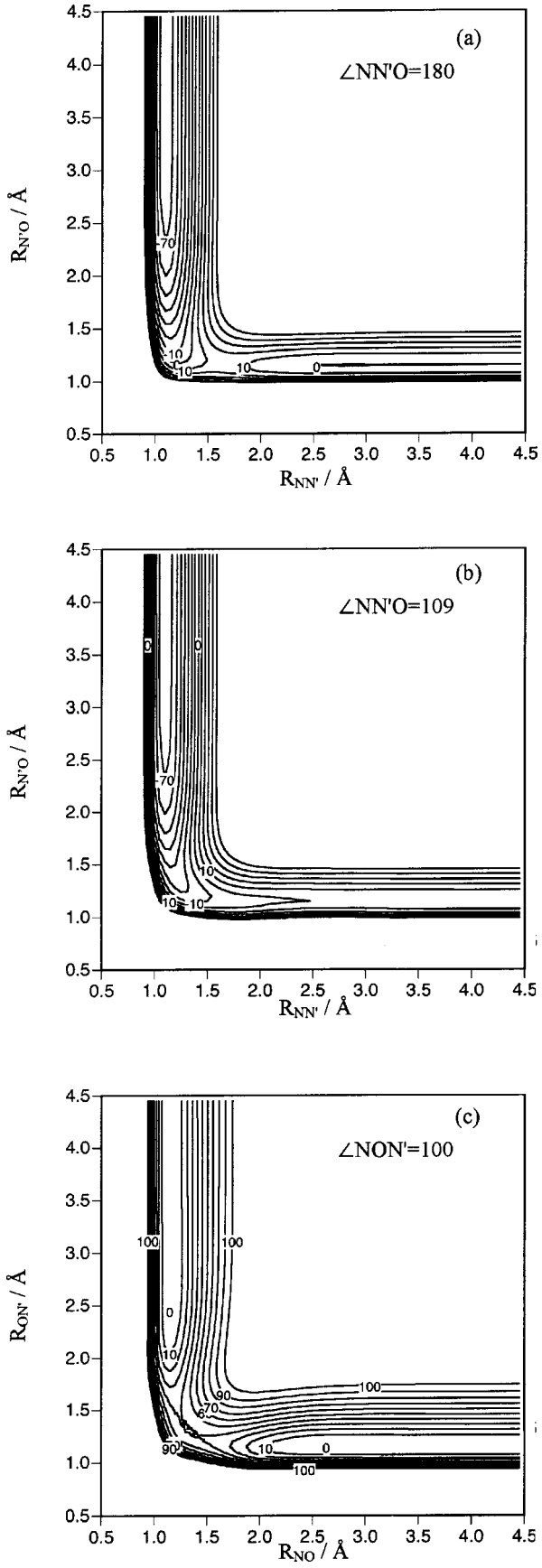

FIG. 3. Equipotential energy contour diagrams of the $^3A''$ analytical PES for $C_{\infty v}$ (a), C_s (b), and C_{2v} (c) geometries. The contours are depicted in increments of 10 kcal/mol, and the zero of energy is taken in reactants [N(^4S) +N′O].

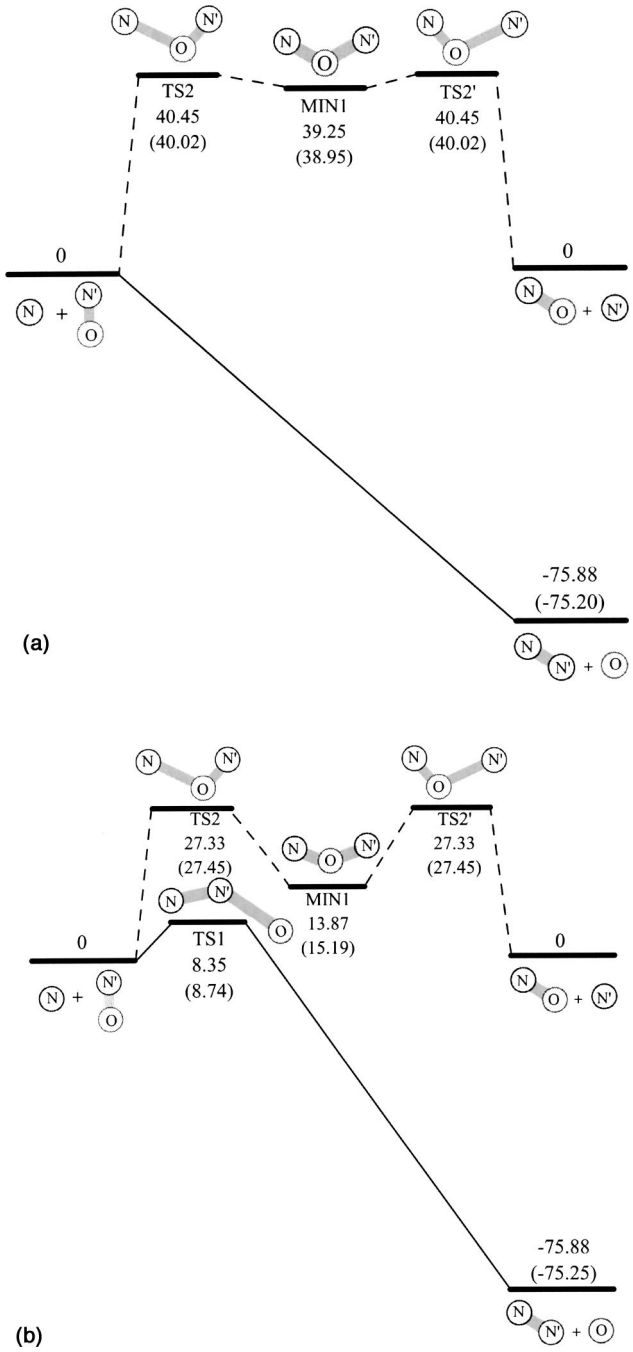

FIG. 4. Schematic representation of the lowest MEP for both the $^3A''$ (a) and the $^3A'$ (b) analytical PESs. Energies are given relative to reactants [N(^4S)+NO] in kcal/mol.

spin-orbit splitting $\Delta(^2\Pi_{3/2}-^2\Pi_{1/2})$ is equal to 121.1 cm^{-1}.[1] The expression for k_1 and k_2 can be obtained from the equation

$$k_i = k_i(^3A'') + k_i(^3A') = \frac{3k_i'(^3A'') + 3k_i'(^3A')}{4(2+2e^{-174.2/T})}, \quad i=1,2. \tag{10}$$

Primed k_i show the rate constants without the inclusion of the electronic partition functions of reactants and the transition state.

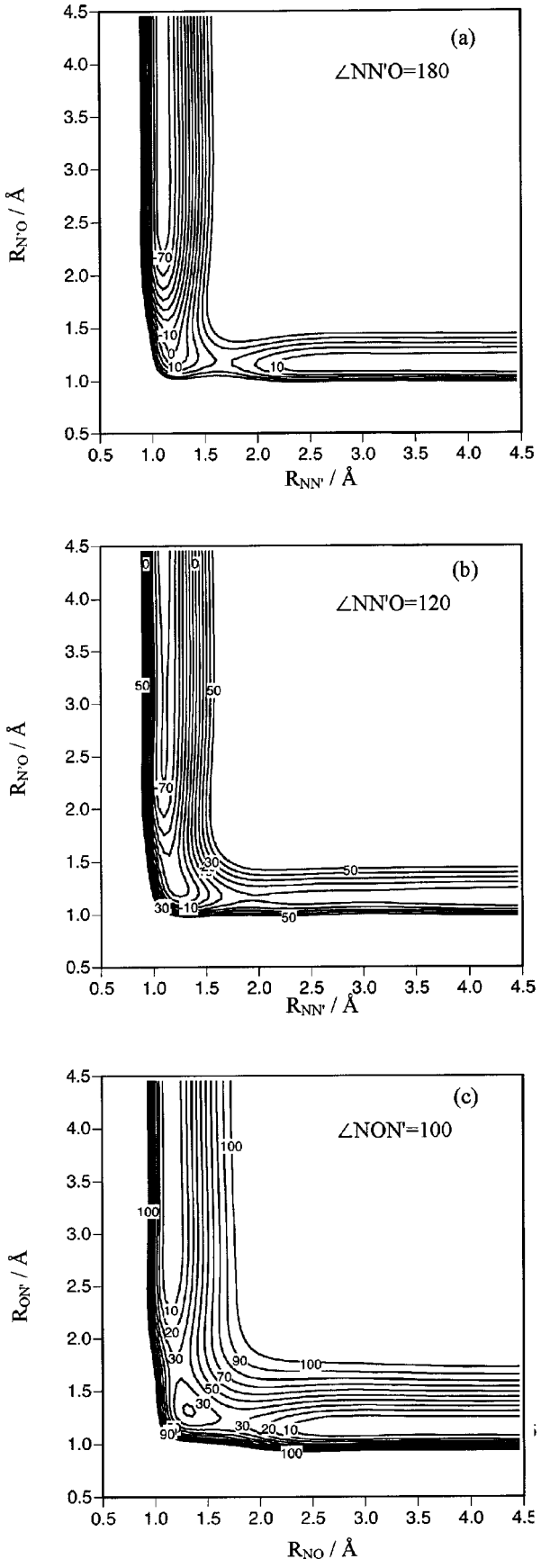

FIG. 5. Equipotential energy contour diagrams of the $^3A'$ analytical PES for $C_{\infty v}$ (a), C_s (b), and C_{2v} (c) geometries. The contours are depicted in increments of 10 kcal/mol, and the zero of energy is taken in reactants [$N(^4S)+N'O$].

Due to the presence of a minimum (MIN1) in the MEP for reaction (2) (Fig. 4), we have considered the following microscopic mechanism to determine its rate constant (k_2):

$$N+N'O \underset{k_{-2a}}{\overset{k_{2a}}{\rightleftarrows}} MIN1 \xrightarrow{k_{2b}} N'+NO, \tag{11}$$

which is more properly applied to the $^3A'$ PES, which presents a more stable minimum and which as well will produce the most important contribution to the total k_2. The application of the steady-state assumption to this type of mechanism[40] will give place to the velocity equation

$$v=\frac{d[NO]}{dt}=\frac{k_{2a}k_{2b}}{k_{-2a}+k_{2b}}[N][N'O]=k_2[N][N'O]. \tag{12}$$

Due to $k_{2b}=k_{-2a}$, the final rate constant k_2 becomes equal to $k_{2a}/2$. Hence VTST calculations determined firstly k_{2a} for each PES before calculating the total k_2. The steady-state approximation is valid for $k_{2a}\ll(k_{-2a}+k_{2b})=2k_{2b}$.[40] We have checked that this condition always fulfills in the present case (e.g., for the $^3A'$ PES, $k_{2b}/k_{2a}>10^{11}$ for all temperatures).

For the reverse reaction (−1), we have also considered the corresponding oxygen atom spin-orbit states ($^3P_2$, $^3P_1$, and $^3P_0$). Thus its electronic partition function is

$$Q^{elec}_{O(^3P)}(T)=g(^3P_2)+g(^3P_1)e^{-\Delta_1/RT}+g(^3P_0)e^{-\Delta_0/RT}, \tag{13}$$

where $g(i)$ represents the electronic degeneracy of each i spin-orbit state, which are equal to 5, 3, and 1, respectively, and Δ_i are the energetic differences between the corresponding i excited electronic state and the ground electronic state, $\Delta_1(^3P_1-^3P_2)$ and $\Delta_2(^3P_0-^3P_2)$, which are equal to 158.27 and 226.98 cm^{-1}, respectively.[1] Therefore, k_{-1} can be determined by the equation

$$k_{-1}=k_{-1}(^3A'')+k_{-1}(^3A') = \frac{3k'_{-1}(^3A'')+3k'_{-1}(^3A')}{(5+3e^{-227.7/T}+e^{-326.6/T})}. \tag{14}$$

Table V shows the calculated VTST rate constants for reaction (1) using the present and previous PESs, comparing also with available experimental data. As was shown in paper I,[24] the estimated complete basis set limit for the energy barrier (TS1) in $^3A'$ PES is 6.74 kcal/mol. Thus a simple scale factor was introduced in the VTST calculations for this PES to better account for this value, instead of the value reproduced by the analytical PES (8.35.kcal/mol). The agreement with the experimental data when considering the new PESs is very good at low and also at very high temperatures. Previous PESs produce poorer rate constants (see Table V), lower by a 10–15 factor at low temperatures and by a 1.2–2.5 factor at high temperatures ($T>1500$ K). Comparing the rate constants arising from each PES, it is appreciated that the effect of the $^3A'$ is certainly minor. The contribution of this latter PES to the total rate constant is small even at high temperatures (e.g., only 10.8% at 2500 K). Therefore, the influence of the inclusion of the scaled barrier is very small.

TABLE V. Theoretical ICVT/μOMT and experimental thermal rate constants for the $N(^4S)+NO(X\,^2\Pi)\rightarrow O(^3P)+N_2(X\,^1\Sigma_g^+)$ reaction.[a]

	$k_1(^3A'')$		$k_1(^3A')$		k_1		
T (K)	New PES	Previous PES[b]	New PES[c]	Previous PES[d]	New PESs[e]	Previous PESs[e]	Experiment[f]
200	6.52×10^{-11}	2.04×10^{-12}	1.38×10^{-19}	1.17×10^{-26}	6.52×10^{-11}	2.04×10^{-12}	4.89×10^{-11}, 3.46×10^{-11}
300	4.68×10^{-11}	2.96×10^{-12}	4.20×10^{-17}	7.30×10^{-22}	4.68×10^{-11}	2.96×10^{-12}	3.75×10^{-11}, 2.93×10^{-11}
400	3.79×10^{-11}	3.79×10^{-12}	7.92×10^{-16}	2.05×10^{-19}	3.79×10^{-11}	3.79×10^{-12}	3.28×10^{-11}, 2.70×10^{-11}
500	3.39×10^{-11}	4.57×10^{-12}	4.85×10^{-15}	6.39×10^{-18}	3.39×10^{-11}	4.57×10^{-12}	
600	3.20×10^{-11}	5.34×10^{-12}	1.68×10^{-14}	6.58×10^{-17}	3.20×10^{-11}	5.34×10^{-12}	
800	3.05×10^{-11}	6.83×10^{-12}	8.40×10^{-14}	1.29×10^{-15}	3.06×10^{-11}	6.83×10^{-12}	
1000	3.02×10^{-11}	8.31×10^{-12}	2.32×10^{-13}	8.10×10^{-15}	3.05×10^{-11}	8.32×10^{-12}	
1250	3.01×10^{-11}	1.01×10^{-11}	5.48×10^{-13}	3.71×10^{-14}	3.07×10^{-11}	1.02×10^{-11}	*3.77×10^{-11}*
1500	3.01×10^{-11}	1.20×10^{-11}	1.00×10^{-12}	1.06×10^{-13}	3.11×10^{-11}	1.21×10^{-11}	4.19×10^{-11}
1750	3.03×10^{-11}	1.38×10^{-11}	1.58×10^{-12}	2.28×10^{-13}	3.19×10^{-11}	1.40×10^{-11}	4.52×10^{-11}
2000	3.07×10^{-11}	1.56×10^{-11}	2.26×10^{-12}	4.17×10^{-13}	3.29×10^{-11}	1.60×10^{-11}	4.78×10^{-11}
2500	3.18×10^{-11}	1.92×10^{-11}	3.87×10^{-12}	9.99×10^{-13}	3.57×10^{-11}	2.02×10^{-11}	5.18×10^{-11}
3000	3.33×10^{-11}	2.28×10^{-11}	5.70×10^{-12}	1.85×10^{-12}	3.90×10^{-11}	2.46×10^{-11}	5.46×10^{-11}
4000	3.67×10^{-11}	3.01×10^{-11}	9.76×10^{-12}	4.25×10^{-12}	4.65×10^{-11}	3.43×10^{-11}	5.83×10^{-11}
5000	4.06×10^{-11}	3.72×10^{-11}	1.41×10^{-11}	7.36×10^{-12}	5.46×10^{-11}	4.46×10^{-11}	*6.06×10^{-11}*

[a]Rate constants are given in $cm^3\,molecule^{-1}\,s^{-1}$. Transmission coefficients κ are equal to 1 for $^3A''$ PES.
[b]Using the PES of Ref. 15 and including the electronic statistical degeneracy factor.
[c]ICVT/μOMT rate constants calculated on the $^3A'$ PES with an scaled energy barrier equal to 6.74 kcal/mol [the *ab initio* CBS limit (Ref. 24)].
[d]Using the PES of Ref. 20 and including the electronic statistical degeneracy factor.
[e]The total theoretical rate constant k_1 is calculated using Eq. (10) and the data of the columns on the left.
[f]Data from Refs. 3 and 9 (200–400 K) and from Ref. 8 (1500–4000 K). Italic numbers show two extrapolated values to allow additional comparison. Errors are indicated in Table I.

For instance, at 2500 K the value of k ($^3A'$, with barrier not scaled) decreases only until 2.83×10^{-12} cm^3 $molecule^{-1}$ s^{-1} (cf. in Table V), which leads to almost the same total rate constant (3.46×10^{-11} $cm^3\,molecule^{-1}\,s^{-1}$). The key improvement in the new theoretical rate constants arises from the new $^3A''$ PES, which gives rate constants higher than the previous PES.[15] In addition, Fig. 6(a) (note the enlarged scale in the k axis) shows the correct change of slope as compared with the experimental data at low[3,9] and high temperatures,[8] not properly described by using previous PESs.

Nevertheless, there are some differences in comparison to another experimental data[2,7] which do not agree with the recommended experimental data,[8,9] although all of them are actually within a relatively small range of k values. The behavior observed at low temperatures for reaction (1) due to the $^3A''$ rate constant is not originated by tunnel effect (in all cases the transmission coefficient κ was equal to 1), as it should be expected for a barrierless reaction, but to the vibrationally adiabatic effective energy barrier derived from the shape of the MEP at each temperature. A slight contribution to the increase of k_1 when the temperature decreases is also originated by the temperature dependence of $Q^{elec}_{NO(^2\Pi)}(T)$. This effect was also reported in a previous study,[18] where QCT thermal rate constants were calculated with a different analytical $^3A''$ PES within the 200–1000 K interval. For these calculations, the introduction of this temperature-dependent statistical degeneracy factor was the only way to produce a positive slope in the Arrhenius plot. Moreover, these QCT rate constants were very similar to the present VTST ones, though for a shorter temperature range. For instance, using their QCT values for the $^3A''$ PES and Eq. (10) [assuming that $k(^3A')$ is negligible for $T<1000$ K] we obtain the following QCT values at 200, 300, and 1000 K: 4.24×10^{-11}, 4.02×10^{-11}, and 3.61×10^{-11} $cm^3\,molecule^{-1}\,s^{-1}$, respectively (cf. Table V). The major shortcoming of this earlier $^3A''$ PES is its rather semiempirical character and inability to describe reaction (2).

Table VI presents the VTST rate constants for reaction (2), which are also displayed in Fig. 6(b). A three-parameter Kooij expression for k_2 was used according to the following equation:

$$k=AT^n e^{B/T}, \tag{15}$$

where A, n, and B are parameters to be optimized by means of a least-squares procedure to fit the rate constants, as is given in Fig. 6(b). For this reaction with an important energy barrier, the small effect of the oxygen spin-orbit states is negligible. In this reaction the main contribution to the total rate constant is due to the $^3A'$ PES, following an opposite behavior as for reaction (1). Although k_2 values are much lower than the k_1 values at low and moderate temperatures ($T<1000$ K), the present results show that the O-abstraction channel accounts for 3.0% of the total reaction [the branching ratio $k_2/(k_1+k_2)$ being expressed in percentage] at 5000 K. This value is equal to the QCT value calculated for the similar reaction but with $N(^2D)$ (Ref. 33) and a much lower temperature (1500 K). The addition of these values at high temperatures is in good agreement with the qualitative accessible experimental information, which indicates that this branching ratio ranges from 0% to 20% when increasing the nitrogen atom translational energy[22,23] [possibly including also $N(^2D)$ and $N(^2P)$]. Although reaction (2) involves heavy atoms, the transmission coefficients κ calculated by the SCT method at different temperatures are high even at room temperature (e.g., 2.58 for $^3A''$ and 1.79 for the $^3A'$ at 300 K) as was also found in similar studies.[35,41]

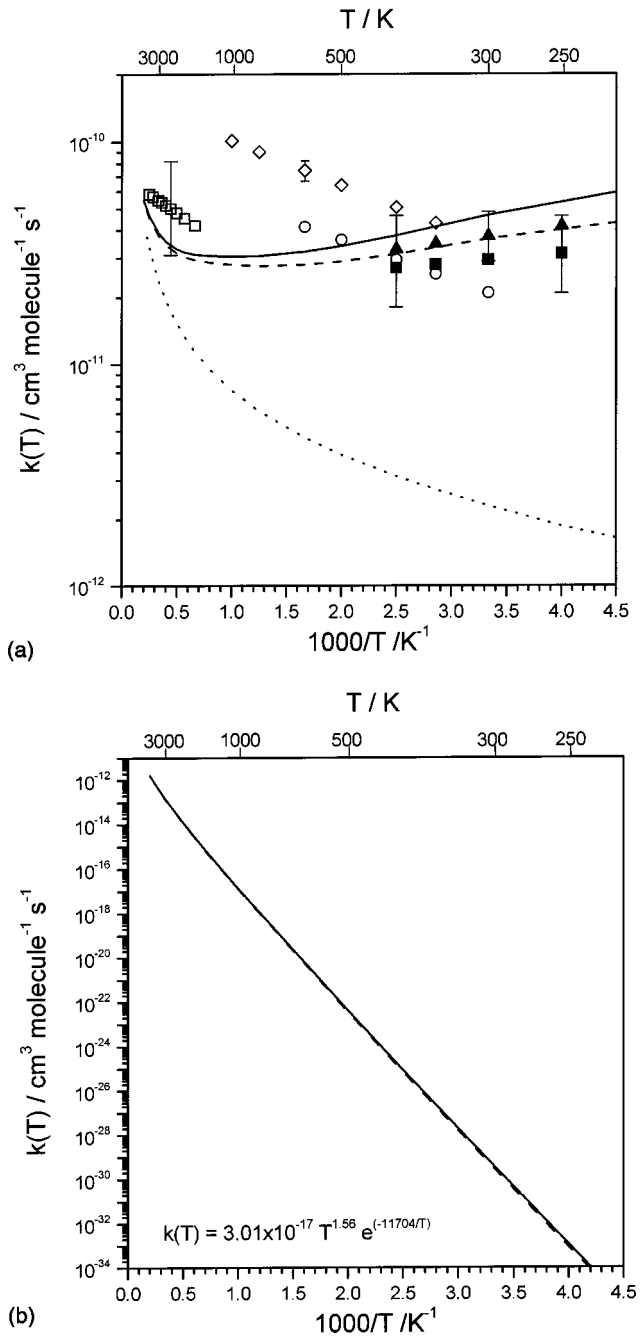

FIG. 6. Arrhenius plots of the calculated and experimental thermal rate constants (250–5000 K) for (a) $N(^4S)+N'O\ (X\ ^2\Pi)\rightarrow O(^3P)+N_2\ (X\ ^1\Sigma_g^+)$ reaction: ICVT/μOMT values with the new analytical PESs with (solid line) and without (dashed line) spin-orbit correction. Dotted line shows the ICVT/μOMT spin-orbit corrected values using the previous PESs (Refs. 15 and 20). Experimental data showing a typical error bar: ○ (Ref. 7), ◇ (Ref. 2), ▲ (Ref. 3), ■ (Ref. 9), and □ (Ref. 8). (b) $N(^4S)+N'O\ (X\ ^2\Pi)\rightarrow N'(^4S)+NO\ (X\ ^2\Pi)$ reaction: ICVT/SCT values with the new analytical PESs with (solid line) and without (dashed line) spin-orbit correction. The *A*, *B*, and *n* optimal parameters [Eq. (15)] fitting the ICVT/μOMT spin-orbit corrected values with the new PESs are also indicated (*k* in $cm^3\,molecule^{-1}\,s^{-1}$).

Finally, we have also computed the thermal rate constants for the reverse reaction (−1) due to the importance of these kinetic data in computational fluid dynamics (CFD) flow simulations for reentry vehicles in Earth's atmosphere. Thus Fig. 7 and Table VII present the thermal rate constants

TABLE VI. Theoretical ICVT/SCT thermal rate constants for the $N(^4S)+N'O(X\ ^2\Pi)\rightarrow N'(^4S)+NO(X\ ^2\Pi)$ reaction.[a]

T (K)	$k_2(^3A'')$	$k_2(^3A')$	k_2[b]
200	5.13×10^{-54}	7.30×10^{-39}	7.30×10^{-39}
300	2.53×10^{-40}	3.31×10^{-30}	3.31×10^{-30}
400	2.38×10^{-33}	8.65×10^{-26}	8.65×10^{-26}
500	4.04×10^{-29}	4.20×10^{-23}	4.20×10^{-23}
1000	1.74×10^{-20}	1.38×10^{-17}	1.38×10^{-17}
1500	1.66×10^{-17}	1.18×10^{-15}	1.20×10^{-15}
2000	5.68×10^{-16}	1.20×10^{-14}	1.26×10^{-14}
3000	2.21×10^{-14}	1.38×10^{-13}	1.60×10^{-13}
4000	1.51×10^{-13}	5.13×10^{-13}	6.64×10^{-13}
5000	5.02×10^{-13}	1.19×10^{-12}	1.69×10^{-12}

[a]Rate constants are given in $cm^3\,molecule^{-1}\,s^{-1}$.
[b]The total theoretical rate constant k_2 is calculated using Eq. (10) and the data of the columns on the left.

for each PES and the total rate constant. An excellent agreement with the experimental data[8] (Table I) is found within the temperature interval 1500–4000 K. The present results with the new PESs also slightly improve the kinetic data derived from previous PESs, as can be seen in Fig. 7. The calculated VTST values are almost independent of the small spin-orbit correction (Fig. 7). VTST rate constants at higher temperatures can also be compared with published QCT (Ref. 20) values derived from our earlier $^3A''$ PES (Ref. 15) and the previous $^3A'$ PES (Ref. 20), including the corresponding statistical degeneracy factor for each PES (i.e., 3/9). This QCT study provided a three-parameter expression

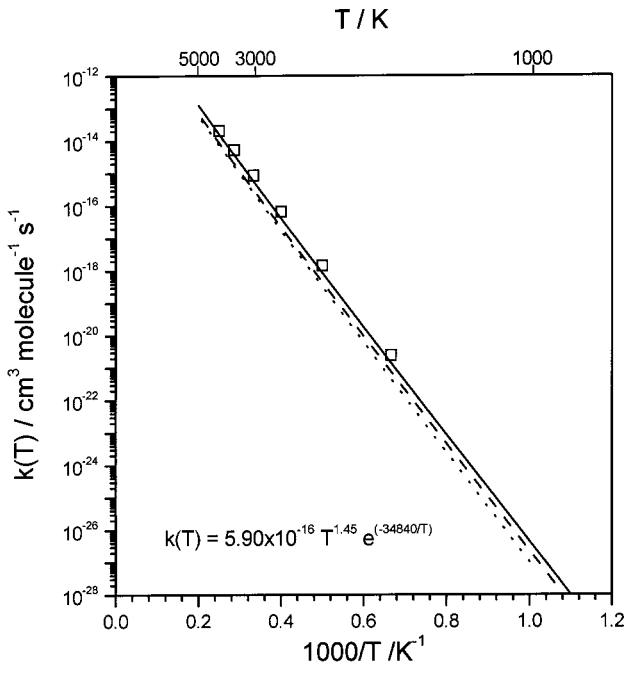

FIG. 7. Arrhenius plots of the calculated and experimental thermal rate constants (1000–5000 K) for the $O(^3P)+N_2\ (X\ ^1\Sigma_g^+)\rightarrow N(^4S)+N'O\ (X\ ^2\Pi)$ reaction: ICVT/μOMT values with the new analytical PESs with (solid line) and without (dashed line) spin-orbit correction. Dotted line shows the ICVT/μOMT spin-orbit corrected values using the previous PESs (Refs. 15 and 20). Experimental data (□) with an error lower than size symbol from Ref. 8. The *A*, *B*, and *n* optimal parameters [Eq. (15)] fitting the ICVT/μOMT spin-orbit corrected values with the new PESs are also indicated (*k* in $cm^3\,molecule^{-1}\,s^{-1}$).

TABLE VII. Theoretical ICVT/μOMT and experimental thermal rate constants for the $O(^3P)+N_2(X\,^1\Sigma_g^+)\rightarrow N(^4S)+NO(X\,^2\Pi)$ reaction.[a]

	$k_{-1}(^3A'')$		$k_{-1}(^3A')$		k_{-1}		
T (K)	New PES	Previous PES[b]	New PES[c]	Previous PES[d]	New PESs[e]	Previous PESs[e]	Experiment[f]
600	5.11×10^{-38}		2.49×10^{-41}		5.12×10^{-38}		
800	3.46×10^{-31}		9.00×10^{-34}		3.46×10^{-31}		
1000	4.44×10^{-27}	1.01×10^{-27}	3.26×10^{-29}	9.92×10^{-31}	4.47×10^{-27}	1.01×10^{-27}	*6.98×10^{-27}*
1500	1.36×10^{-21}	4.50×10^{-22}	4.39×10^{-23}	3.96×10^{-24}	1.41×10^{-21}	4.47×10^{-22}	2.44×10^{-21}
2000	7.78×10^{-19}	3.29×10^{-19}	5.57×10^{-20}	8.74×10^{-21}	8.33×10^{-19}	3.20×10^{-19}	1.45×10^{-18}
2500	3.61×10^{-17}	1.80×10^{-17}	4.27×10^{-18}	9.37×10^{-19}	4.03×10^{-17}	1.71×10^{-17}	6.66×10^{-17}
3000	4.76×10^{-16}	2.70×10^{-16}	7.95×10^{-17}	2.19×10^{-17}	5.56×10^{-16}	2.48×10^{-16}	8.56×10^{-16}
3500	3.06×10^{-15}	1.91×10^{-15}	6.56×10^{-16}	2.13×10^{-16}	3.72×10^{-15}	1.70×10^{-15}	5.31×10^{-15}
4000	1.25×10^{-14}	8.44×10^{-15}	3.25×10^{-15}	1.19×10^{-15}	1.58×10^{-14}	7.24×10^{-15}	2.08×10^{-14}
5000	9.27×10^{-14}	7.02×10^{-14}	3.15×10^{-14}	1.39×10^{-14}	1.24×10^{-13}	5.64×10^{-14}	*1.41×10^{-13}*

[a]Rate constants are given in cm^{-3} $molecule^{-1}$ s^{-1}. Transmission coefficients κ are equal to 1 for $^3A''$ PES.
[b]Using the PES of Ref. 15 and including the electronic statistical degeneracy factor.
[c]ICVT/μOMT rate constants calculated on the $^3A'$ PES with a scaled energy barrier [for reaction (1)] equal to 6.74 kcal/mol [the *ab initio* CBS limit (Ref. 24)].
[d]Using the PES of Ref. 20 and including the electronic statistical degeneracy factor.
[e]The total theoretical rate constant k_{-1} is calculated using Eq. (14) and the data of the columns on the left.
[f]Data from Ref. 8 (1500–4000 K). Italic numbers show two extrapolated values to allow further comparison. Errors are indicated in Table I.

of $k_{-1}(T)=(9.45\pm0.32)\times10^{-12}\times T^{0.42}\times e^{-42938\pm147/T}$ cm^3 $molecule^{-1}\,s^{-1}$ for the 3000–20 000 K range. Using this equation, we obtain the values of 1.66×10^{-16}, 6.70×10^{-15}, and 6.30×10^{-14} $cm^3\,molecule^{-1}\,s^{-1}$ for 3000, 4000, and 5000 K, respectively. These QCT results are consistent with the calculated VTST results using these same PESs (Table VII), which are worse than the present ones, particularly for higher temperatures. At 5000 K the reported QCT $k(^3A'')/k(^3A')$ ratio[20] was 15 as compared with the VTST value of 5.1 for both previous PESs, which differ from the small value (2.9) obtained with the new PESs. Therefore, we conclude that the excited PES ($^3A'$) must be included in kinetic and dynamic studies of reaction (-1) at temperatures lower than those predicted in the QCT study ($T>8000$ K). Whereas the QCT $k_{-1}(^3A'')/k_{-1}(^3A')$ ratio is 2 at 12 000 K, the same VTST value with the new PESs is obtained at 7800 K.

QCT and quantum wave-packet dynamic studies using these new PESs are in progress in our group to provide more detailed information of the kinetics and dynamics of all reaction channels.

IV. CONCLUSIONS AND REMARKS

In this work we have built new analytical fits of the ground PES ($^3A''$) and the excited PES ($^3A'$) involved in the $N(^4S)+NO(X\,^2\Pi)$ reaction [N-abstraction (1) and O-abstraction (2) channels] and also for the reverse, (-1), using *ab initio* data reported in paper I (Ref. 24) along with new extensive grids of high-level *ab initio* points [CASPT2(10,9) G2/cc-pVTZ calculations] computed in the present work. Diatomic D_e and R_e spectroscopic data were also introduced to better account for the exoergicity of reaction (1). The final RMSD for the $^3A''$ surface was equal to 1.44 kcal/mol for the NN′O region and 2.59 kcal/mol for the NON′ region, with a global RMSD of 1.80 kcal/mol. For the $^3A'$ surface, we obtained a final RMSD equal to 1.61 kcal/mol for the NN′O region and 2.85 kcal/mol for the NON′ region, with a global RMSD of 2.28 kcal/mol. These RMSDs were well below the estimated *ab initio* errors.

Thermal rate constants were calculated for both direct reaction channels and for the reverse reaction by means of the variational transition-state theory with the inclusion of a semiclassical tunneling correction. Theoretical rate constants for reaction (1) were in excellent agreement with experimental data at low to moderate and also at very high temperatures (200–5000 K), significantly improving the results obtained by using previous PESs. The contribution of the $^3A'$ PES to the total rate constant was small even at high temperatures (e.g., only 10.8% at 2500 K). The main enhancement in the rate constants arises from the new $^3A''$ PES, which gives rate constants higher than the previous PES.

The VTST calculation for reaction (2) showed that the main contribution to the total rate constant was due to the $^3A'$ PES, differing from the behavior in reaction (1). Despite k_2 values much lower than k_1 values at low and moderate temperatures ($T<1000$ K), the present results have shown that the O-abstraction channel accounts for 3.0% of the total reaction at 5000 K, which is consistent with the limited available experimental information, which indicates that the branching ratio $[k_2/(k_1+k_2)]$ should be between 0% and 20%, depending on the N-atom translational energy.

Calculated VTST rate constants for the reverse reaction (-1) were also in very good agreement with the experimental data within the temperature interval 1500–5000 K. The present results with the new PESs also improved slightly the kinetic data derived by using the previous PESs. Hence the $^3A'$ PES should be included in kinetic and dynamic studies of this reverse reaction for temperatures much lower than those predicted in previous QCT studies, although its contribution to the total k_{-1} is low (e.g., 6.7% at 2000 K).

The new analytical PESs accurately describe the NNO C_s regions and also the NON C_{2v} and C_s regions, which make them valuable for use in theoretical studies of all three reaction processes. Dynamic and kinetic studies with the new PESs using the QCT method and a quantum wave-packet

dynamic approach are in progress in our group to further study the reactions (1) and (2), especially regarding the dynamical properties derived from each PES.

ACKNOWLEDGMENTS

This work has been supported by the Spanish Ministry of Education and Culture (Project No. PB98-1209-C02-01) and the Spanish Ministry of Science and Technology (Project Nos. BQU2002-03351 and BQU2002-04269-C02-02). Financial support from the European Union (INTAS Project No. 99-00701) and the ''Generalitat'' (Autonomous Government) of Catalonia (Project No. 2001SGR 00041) is also acknowledged. P.G. thanks the ''Universitat de Barcelona'' for a predoctoral research grant. The authors are grateful to the ''Center de Computació i Comunicacions de Catalunya (C^4-CESCA/CEPBA)'' for providing part of the computer time.

[1] M. W. Chase, Jr., C. A. Davies, J. R. Downey, Jr., D. J. Frurip, R. A. McDonald, and A. N. Syverud, J. Phys. Chem. Ref. Data Suppl. **14**, 1 (1985).
[2] D. E. Siskind and D. W. Rusch, J. Geophys. Res. **97**, 3209 (1992).
[3] P. O. Wennberg, J. G. Anderson, and D. K. Weisenstein, J. Geophys. Res. **99**, 18 839 (1994).
[4] P. Warneck, *Chemistry of the Natural Atmosphere* (Academic, San Diego, 1998), Chap. 3.
[5] G. Marston, Chem. Soc. Rev. **25**, 33 (1996).
[6] T. Kurotaki, AIAA paper No. 2000-2366, 2000.
[7] M. A. A. Clyne and I. S. McDermid, J. Chem. Soc., Faraday Trans. 1 **71**, 2189 (1975).
[8] D. L. Baulch, C. J. Cobos, R. A. Cox, G. Hayman, Th. Just, J. A. Kerr, T. Murrells, M. J. Pilling, J. Troe, R. W. Walker, and J. Warnatz, J. Phys. Chem. Ref. Data **23**, 847 (1994).
[9] W. B. DeMore, D. M. Golden, R. F. Hampson, M. J. Kurylo, C. J. Howard, A. R. Ravishankara, C. E. Kolb, and M. J. Molina, *Chemical Kinetics and Photochemical Data for Use in Stratospheric Modelling*, Evaluation 12, JPL Publ. 97-4 (Jet Propulsion Laboratory, Pasadena, CA, 1997).
[10] G. Black, R. L. Sharpless, and T. G. Slanger, J. Chem. Phys. **58**, 4792 (1973).
[11] J. E. Morgan and H. I. Schiff, Can. J. Phys. **41**, 903 (1963).
[12] J. E. Morgan, L. F. Phillips, and H. I. Schiff, Discuss. Faraday Soc. **33**, 118 (1962).
[13] M. Gilibert, A. Aguilar, M. González, F. Mota, and R. Sayós, J. Chem. Phys. **97**, 5542 (1992).
[14] S. P. Walch and R. L. Jaffe, J. Chem. Phys. **86**, 6946 (1987); AIP Document No. PAPSJCPSA-86-6946-10.
[15] M. Gilibert, A. Aguilar, M. González, and R. Sayós, J. Chem. Phys. **99**, 1719 (1993).
[16] A. Aguilar, M. Gilibert, X. Giménez, M. González, and R. Sayós, J. Chem. Phys. **103**, 4496 (1995).
[17] R. Sayós, A. Aguilar, M. Gilibert, and M. González, J. Chem. Soc., Faraday Trans. 1 **89**, 3223 (1993).
[18] J. W. Duff and R. D. Sharma, Geophys. Res. Lett. **23**, 2777 (1996).
[19] J. W. Duff and R. D. Sharma, Chem. Phys. Lett. **265**, 404 (1997).
[20] D. Bose and G. V. Candler, J. Chem. Phys. **104**, 2825 (1996).
[21] D. Bose and G. V. Candler, J. Thermophys. Heat Transfer **10**, 148 (1996).
[22] J. Dubrin, C. Mackay, and R. Wolfgang, J. Chem. Phys. **44**, 2208 (1966).
[23] R. Iwata, A. Ferrieri, and A. P. Wolf, J. Phys. Chem. **90**, 6722 (1986).
[24] P. Gamallo, M. González, and R. Sayós, J. Chem. Phys. **118**, 10602 (2003).
[25] B. O. Roos, P. R. Taylor, and P. E. M. Siegbahn, Chem. Phys. **48**, 157 (1980).
[26] B. O. Roos, in *Advances in Chemical Physics: Ab Initio Methods in Quantum Chemistry—II*, edited by K. P. Lawley (Wiley, Chichester, 1987), Vol. LXIX, p. 399.
[27] T. H. Dunning, Jr., J. Chem. Phys. **90**, 1007 (1989).
[28] K. Andersson, Theor. Chim. Acta **91**, 31 (1995).
[29] K. Andersson, M. R. A. Blomberg, M. P. Fülscher *et al.*, computer code MOLCAS 4.1, Lund University, Sweden, 1998.
[30] J. N. Murrell, S. Carter, S. C. Farantos, P. Huxley, and A. J. C. Varandas, *Molecular Potential Energy Surfaces* (Wiley, New York, 1984).
[31] M. González and R. Sayós, computer code DIATOMFIT (unpublished).
[32] R. Sayós and M. González, computer code SM3FIT (unpublished).
[33] M. González, R. Valero, and R. Sayós, J. Chem. Phys. **113**, 10 983 (2000).
[34] M. González, I. Miquel, and R. Sayós, J. Chem. Phys. **115**, 2530 (2001).
[35] R. Sayós, C. Oliva, and M. González, J. Chem. Phys. **117**, 670 (2002).
[36] K. P. Huber and G. Herzberg, *Molecular Spectra and Molecular Structure IV. Constants of Diatomic Molecules* (Van Nostrand Reinhold, New York, 1979).
[37] R. Sayós, C. Oliva, and M. González, J. Chem. Phys. **115**, 1287 (2001).
[38] D. G. Truhlar, B. C. Garrett, and S. J. Klippenstein, J. Phys. Chem. **100**, 12 771 (1996).
[39] R. Steckler, Y. Chuang, E. L. Coitiño, W. Hu, Y. Liu, G. C. Lynch, K. A. Nguyen, C. F. Jackels, M. Z. Gu, I. Rossi, P. Fast, S. Clayton, V. S. Melissas, B. C. Garrett, A. D. Isaacson, and D. G. Truhlar, computer code POLYRATE, version 7.0, Department of Chemistry and Supercomputer Institute, University of Minnesota, 1996.
[40] G. I. Gellene, J. Chem. Educ. **72**, 196 (1995).
[41] R. Sayós, J. Hijazo, M. Gilibert, and M. González, Chem. Phys. Lett. **284**, 101 (1998).